Hybrid magnetic skyrmion

H. Z. Wu,[1] B. F. Miao,[1,2] L. Sun,[1,2] D. Wu,[1,2] and H. F. Ding[1,2,*]

[1]*National Laboratory of Solid State Microstructures and Department of Physics, Nanjing University, 22 Hankou Road, Nanjing 210093, P.R. China*

[2]*Collaborative Innovation Center of Advanced Microstructures, Nanjing University, 22 Hankou Road, Nanjing 210093, P.R. China*

(Received 8 November 2016; revised manuscript received 20 April 2017; published 11 May 2017)

We introduce the concept of the hybrid magnetic skyrmion (HMS) by patterning arrays of magnetic nanodisks on top of thin films that possess the Dzyaloshinskii-Moriya interaction (DMI). The practical feasibility of the method is validated by micromagnetic simulations and computed Skyrmion number per unit cell. The HMS has enhanced stability and mobility with respect to existing skyrmion configurations. The skyrmion Hall effect is substantially reduced, in comparison with skyrmion stabilized by the DMI only. We created isolated skyrmions via current pulses and drove them by a continuous current at enhanced speed of 750 m/s.

DOI: 10.1103/PhysRevB.95.174416

Magnetic skyrmions possess a nontrivial spin texture and carry a topological charge [1]. They are relatively stable and inert under small perturbations due to the topological protection. Since the first observation of magnetic skyrmions in bulk magnets with broken inversion symmetry [2], there has been considerable attention due to their fundamental interest and potential for applications [3–13]. For instance, skyrmions are promising candidates for future information technology due to their small size and to the small current densities needed to displace them [14–16]. Also, in contrast to domain walls, the flexibility of skyrmions allows them to be less hindered by defects [14,17,18]. Skyrmion states are generally explained by the existence of the Dzyaloshinskii-Moriya interaction (DMI) in systems lacking inversion symmetry. Skyrmions were typically found to be stable at low temperature in magnetic fields, which impedes their physical exploration and application [2–4]. Although major effort has been made to extend the phase diagram to higher temperatures, it was only recently that DMI-induced, room temperature skyrmions were reported [19–24]. As the DMI is commonly weak, there is only a small group of materials where skyrmions arise naturally from the inherent DMI [natural skyrmion materials, Fig. 1(a)]. Alternatively, there is a growing group of artificially designed magnetic superstructures that enable the existence of skyrmions without the need of a microscopically built-in DMI mechanism [artificial skyrmion materials, Fig. 1(b)] [25,26]. Such artificial skyrmion crystals have been realized experimentally at room temperature [27–29]. Numerical simulations also suggest artificial skyrmion crystals have similar dynamic behavior to that of the natural skyrmion crystal derived from the DMI [30,31]. Artificial skyrmions, without the limitation of a DMI, significantly expand the pool of prospective materials for skyrmion-based systems. The mobility of the artificial skyrmion, however, is restricted by the patterned disks.

Another interesting phenomenon associated with skyrmion is the skyrmion Hall effect [14,32]. Owning to its specific magnetic configuration, skyrmion does not only move forward but also rotates when it is driven by a spin-polarized current. This leads to a transverse movement besides the motion along the current direction, similar as the Hall effect [33]. The effect, however, significantly limits the speed of the skyrmion motion as the skyrmion can be driven out of the track when a high current is used, resulting in a loss of information. To achieve a high-speed skyrmion-based spintronics device, the skyrmion Hall effect needs to be suppressed effectively [32].

Herein, we present the concept of the hybrid magnetic skyrmion (HMS), which is based on the advantages of both natural and artificial skyrmion materials. A natural approach to seek an improvement beyond what each of the components can give separately would be to stack the natural and the artificial skyrmion crystals on each other in close proximity. This leads to an increase in stability, but the skyrmion mobility is compromised. By inserting a spacer with suitable thickness, we decouple the two original materials from direct coupling to RKKY-type. Remarkably, we find that not only the skyrmion mobility is significantly increased but also the skyrmion Hall effect is effectively suppressed due to the attraction of the skyrmion by the disks. The proposed HMS can be driven by an electrical current to a speed of 750 m/s, which is two times larger than the skyrmion with DMI only. We further demonstrate the viability of information encoding and propagation with the HMS in a nanotrack. With a vertically injected current pulse, isolated skyrmions can be created due to the spin transfer torque effect [34,35]. With a steady current, the skyrmions can then be driven with relatively high speed. As individual skyrmion can be detected by a simple Hall geometry via the topological Hall effect [9,36,37], the proposed hybrid structure enables the construction of the HMS racetrack memory that can work at high temperature and with high speed.

There are two types of DMI, the bulk-type and the interfacial-type. Typically, the bulk-type DMI favors the formation of Bloch-type (vortex-type) skyrmions, while the interfacial DMI results in Néel-type skyrmions. Here, we focus on the simulations of bulk-type DMI-induced skyrmions. The Hamiltonian of the DMI term can be written as $H_{\mathrm{DM}} = -\vec{D}_{12} \cdot (\vec{S}_1 \times \vec{S}_2)$, where the Dzyaloshinskii-Moriya vector $\vec{D}_{12}$ is parallel with the unit vector joining spin $\vec{S}_1$ and $\vec{S}_2$ [See the inserted sketch in Fig. 1(a)]. The spin rotates along the plane perpendicular to the radial direction and forms a Bloch-type skyrmion. Figure 1(a) presents a schematic of

*hfding@nju.edu.cn

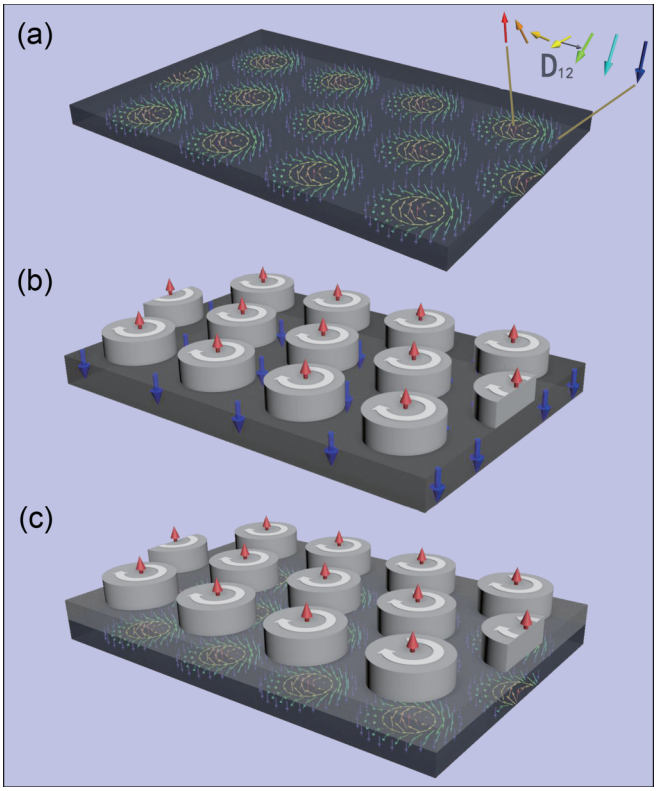

FIG. 1. (a) Schematic of the spin configuration in a Bloch-type, DMI-induced skyrmion crystal with arrows representing direction of local moments. The DMI vector $\vec{D}_{12}$ is parallel to the direction joining neighboring sites. (b) Schematic of an artificial skyrmion crystal, with ordered arrays of vortices on top of a film with perpendicular anisotropy. (c) The proposed HMS crystal, in which ordered arrays of vortices are placed on top of a film with DMI. The exchange coupling of the capping vortices stabilizes the skyrmion crystal beneath.

a Bloch-type skyrmion crystal with hexagonal symmetry, where the arrows represent the direction of the local moment. Typically, this type of skyrmion crystal only exists at low temperature and under a magnetic field. On the other hand, artificial skyrmion crystal can be realized at higher temperature via patterning an array of magnetic vortices onto the surface of a perpendicularly magnetized film [Fig. 1(b)].

By patterning arrays of magnetic disks onto a substrate with DMI, we show the concept of the HMS [Fig. 1(c)]. Remarkably, the hybrid has a significantly enhanced stability in comparison with skyrmions stabilized with only a DMI of the same magnitude. With proper tuning of the exchange coupling between the film and the disks, the skyrmions beneath can be moved by a spin-polarized current. Thus, HMS benefit from both the advantages of the natural DMI-induced skyrmion and the artificial skyrmion.

The micromagnetic simulations are performed via the OOMMF code, including a bulk-type DMI [38] and the thermal fluctuations [39]. For the calculation of all temperature- and field-dependences of topological charge density, the dimensions of the magnetic substrate with DMI are $210 \times 240 \times 1\,\mathrm{nm}^3$ with cell size $2 \times 2 \times 1\,\mathrm{nm}^3$. Material parameters are used for FeGe in the calculations as follows: experimentally reported temperature dependent saturation magnetization [40] and $M_{\mathrm{sub}} = 3.3 \times 10^5\,\mathrm{A/m}$ at 0 K. The exchange constant $A_{\mathrm{sub}} = 7.54 \times 10^{-12}\,\mathrm{J/m}$, is calculated from Curie temperature. Similar approach has been used in Ref. [41]. The DMI constant $D = 1.35\,\mathrm{mJ/m}^2$ is determined from the helical period 70 nm [42]. We also include perpendicular magnetocrystalline anisotropy $K_u = 1.5 \times 10^5\,\mathrm{J/m}^3$. As FeGe is 1-nm thick, the magnetic anisotropy may originate from the surface anisotropy and/or the magnetoelastic anisotropy caused by the lattice mismatch *etc*. In the calculations for the HMS, an array of vortex disks with 60-nm diameter, 70-nm disk spacing, and 4-nm thickness are patterned onto the DMI material. The saturation magnetization and exchange constant are $M_{\mathrm{disk}} = 1.4 \times 10^6\,\mathrm{A/m}$ and $A_{\mathrm{disk}} = 2.5 \times 10^{-11}\,\mathrm{J/m}$ (corresponding to the values of Co), respectively. The coupling between the disks and DMI substrate changes depending on the geometry (see below).

For simulations of the spin transfer torque with current-in-plane geometry, we consider both adiabatic and nonadiabatic terms in the Landau-Lifshitz-Gilbert equation: $\tau_{\mathrm{adiab.}} = u\mathbf{m} \times (\mathbf{m} \times \frac{\partial \mathbf{m}}{\partial x})$ and $\tau_{\mathrm{nonadiab.}} = \beta u(\mathbf{m} \times \frac{\partial \mathbf{m}}{\partial x})$, where $u = \gamma(\hbar j P/2eM_{\mathrm{S}})$, x is the direction of the electron velocity, γ is the gyromagnetic ratio, M_{S} is the saturation magnetization, j is the current density, P is the spin polarization, and β is the nonadiabatic damping coefficient [43,44]. In the simulation, the Gilbert damping coefficient α is set to 0.05, and the nonadiabatic damping β is set to 0.08. Current flows only within the film with DMI. For the simulation of the nucleation of skyrmions with vertically injected spin polarized current, we consider the in-plane torque written as $\tau_{IP} = \frac{u}{t}\mathbf{m} \times (\mathbf{m}_P \times \mathbf{m})$, where $\mathbf{m}_p$ is the current polarization vector, and t is the FeGe thickness. In the calculation, the out-of-plane field-like torque is set to zero.

Figure 2 shows the comparison of the stability of the skyrmion before and after capping with the magnetic disks. In Fig. 2(a), we present temperature dependent snapshots of the magnetic configuration for a 1-nm FeGe film with DMI. The system was originally relaxed from the random state. At 0 K, a hexagonal skyrmion lattice is formed when a 250 mT field is applied normal to the film plane. The skyrmion size (defined as the diameter of the line where $m_z = 0$) is ~40 nm with a ~70−nm lattice spacing in good agreement with the experimentally reported value [6]. With increasing temperature, the hexagonal order and the skyrmion itself distort due to thermal fluctuations. Also, the background becomes blurred and no skyrmion can be found above 280 K. In contrast, the system after capping with the disk array (60 nm in diameter and 70 nm in spacing) shows strongly enhanced stability, where the skyrmion configuration shows no apparent change up to 275 K. We note that, strictly speaking, the micromagnetic approach provides a correct description of magnetic systems only for low temperatures [45]. Thereby, the topological charge dependencies shown in Figs. 2(c), 2(d), and Fig. 3(d) serve only as a rough estimation of the predicted effect of the enhancement of the skyrmion phase. A more precise estimation of the temperature effects could be achieved with atomistic models based on Monte Carlo simulations [46,47] or with an advanced micromagnetic approach adapted for high temperatures and based on the Landau-Lifshitz-Bloch equation [48,49].

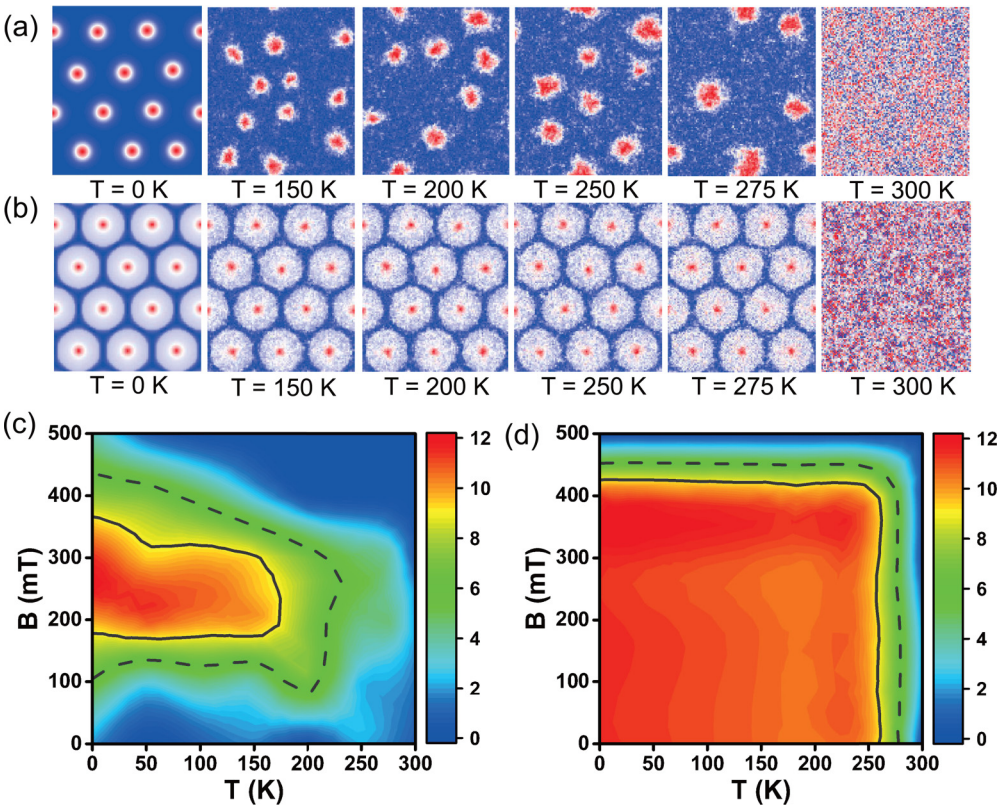

FIG. 2. Temperature-dependent snapshots of the magnetic configuration of the film with DMI only (a) and the film with DMI and capping disk (b). Red/blue represents moment pointing out-of-plane/into-the-plane, respectively. Image sizes are $210 \times 240\,\mathrm{nm}^2$. Temperature- and field-dependence of S in the thin film (c) without capping vortices and (d) with capping vortices. The stability is greatly enhanced in the latter case. Solid/dash lines in (c) and (d) represent isolines with topological number of 80% and 50% of the maximum value, respectively.

In order to compare the stability quantitatively, we compute the integrated skyrmion number $S = \frac{1}{4\pi}\int m \cdot (\frac{\partial m}{\partial x} \times \frac{\partial m}{\partial y})dxdy$ [2,14,50]. The temperature- and field-dependence of S of a 1-nm FeGe film with DMI (without capping) is summarized in Fig. 2(c), which is similar to that reported by Huang et al [8]. As a skyrmion unit possesses a skyrmion number S of 1 or -1 (in our case, $S = 1$), an ordered skyrmion crystal would have $S = 12$ for such a given area [red region in Fig. 2(c)]. To better illustrate the temperature- and field-dependence of S, we define two boundaries where the skyrmion number of the given area has 80% (solid line) and 50% (dash line) of the maximum value. The skyrmion crystal without capping disks is stable only between 180 and 350 mT and <180 K with the 80%-boundary definition. In comparison, the area with large value of S for the system after capping with disk array is greatly extended [Fig. 2(d)]. Given the same definition of an 80% boundary, the skyrmion phase is stable for $0-420$ mT and <260 K, which is significantly larger than that without a disk capping. We, thus, demonstrate that the vortex patterning onto the magnetic material with DMI can indeed enhance significantly the stability of the skyrmion crystal beneath.

As has been reported, DMI-induced skyrmions can be moved at low current density via the spin transfer torque mechanism. Thus, they have been proposed as candidates for information carriers [14–16]. As a reference, we first compute the current-driven motion of skyrmions in a nanotrack without capping disks. The dimension of the nanotrack is $1400 \times 100 \times 1\,\mathrm{nm}^3$. An in-plane current of spin polarization $P = 0.4$ is injected with electron flow along the nanotrack. We find that the current threshold is small, well below $1.0 \times 10^{10}\,\mathrm{A/m}^2$, and the velocity is linearly proportional to the injected current density [blue triangles in Fig. 3(a)], similar to previous findings [14]. Under a current density of $4.0 \times 10^{12}\,\mathrm{A/m}^2$, skyrmions can reach a velocity of $\sim$320 m/s. Upon further increasing the current density, we find that the skyrmion will deviate from the center of the track and slip away at the edge of the track due to the skyrmion Hall effect [see blue triangles in Fig. 3(b)], in agreement with previous findings [14,32]. Hence, the velocity is limited.

As a comparison, we also computed the current-driven dynamics for the skyrmion with disk capping. As mentioned above, the stability of a skyrmion crystal with disk capping is extended, but its mobility is compromised, as is the case for the artificial skyrmion [25]. To remove this obstacle, we reduced the magnetic coupling between the film with DMI and the vortices by inserting a nonmagnetic spacer in between. In such a configuration, the magnetic coupling changed from direct coupling to RKKY-type whose strength can be tuned by varying the spacer thickness [51,52]. The typical maximum value for the ferromagnetic (FM) coupling is of the order of $10^{-4}\,\mathrm{J/m}^2$ [51,53,54]. In our simulations, we inserted 6-nm Cu and choose the RKKY coupling strength to be $A_{\mathrm{RKKY}} = 4.0 \times 10^{-5}\,\mathrm{J/m}^2$. Remarkably, we find that

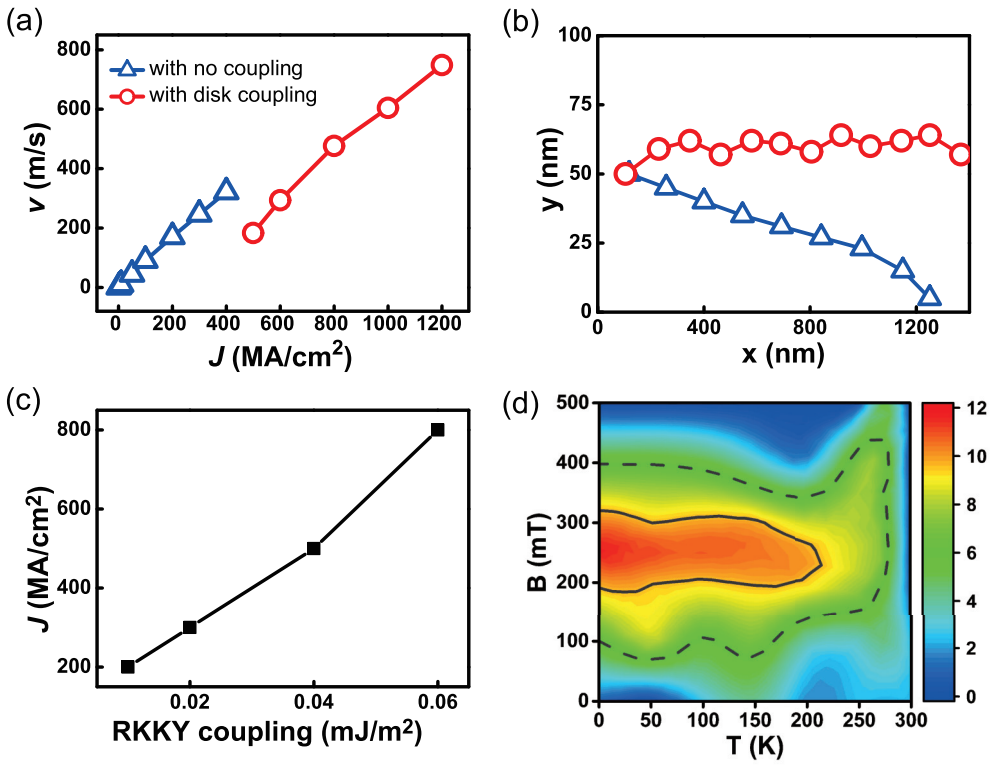

FIG. 3. (a) Skyrmion velocity v as a function of in-plane current density J for skyrmions with DMI only (blue triangle) and the HMS with magnetic disks lifted above (red circle). The velocity of skyrmions with DMI only is limited by the skyrmion Hall effect. (b) The trajectories for skyrmion with DMI only and HMS driven by current with 1.0×10^{13} A/m, respectively. Time interval for neighboring position is set as 0.1 ns. (c) The threshold current that enables skyrmion motion versus the RKKY coupling strength between magnetic disk and DMI material. (d) Temperature- and field-dependence of S of the HMS with lifted magnetic disks. Solid/dash line represents isolines with topological number of 80% and 50% of the maximum value, respectively.

skyrmions stabilized with this configuration can be moved when the current is $>5.0 \times 10^{12}$ A/m^2. Above that, the velocity of the skyrmions show a linear dependence with slope similar to that without vortex capping [red circles in Fig. 3(a)]. Equally interesting, we find that the vortex can also serve as an attracting center, significantly reducing the skyrmion Hall effect [14,32,55]. Thus, the skyrmion can be moved with speed up to 750 m/s, which is two times the speed of the skyrmion without vortex capping. Figure 3(b) presents the trajectories for DMI-induced skyrmion and HMS under current with density of 1.0×10^{13} A/m^2, respectively. The time interval for neighboring position is 0.1 ns. Obviously, the skyrmion Hall effect of DMI-induced skyrmion is strongly suppressed in the HMS system. With this current density, skyrmion moves at the speed of 600 m/s which results in a reading speed of 8 Gb/s for a single track, given that the separation between each skyrmion is ~70 nm. One can expect that the reading speed can be readily increased when multiple tracks are used simultaneously. We also calculate the relationship between the lowest current needed to drive the HMS and the RKKY coupling strength. The result presented in Fig. 3(c) clearly indicates that higher threshold current is needed when RKKY coupling strength increases. In addition, the skyrmion state is stable within (190 mT, 310 mT) and below 220 K in this geometry [Fig. 3(d)], which is extended by 25% compared with the skyrmion phase without vortex capping [Fig. 2(c)]. We note here that the simulations are for Co disks on an FeGe film but the generality of the method is not limited to these materials. Since the swirling spin structure of the disk and the interlayer exchange coupling favor the stability of the skyrmion, similar effect would be expected for other materials. We applied our method for Co disks on an $Fe_{0.5}Co_{0.5}Si$ and found similar results. Our method would be especially useful for the DMI induced skyrmion material with the phase stability close to room temperature.

For a skyrmion-based information technology, controllable creation, manipulation, and detection of the skyrmion are necessary. We demonstrate that skyrmions can be nucleated and driven steadily in a prototype skyrmion-based racetrack memory. The detection of skyrmions can be achieved by the measurement of the topological Hall effect, as has been reported previously [see Fig. 4(a)] [9,36]. The film with DMI is relaxed from saturation state at -250 mT along $-z$ direction, and the capping disks are in vortex states with $+z$ polarity and counterclockwise circulation. A vertical spin polarized current pulse is injected through a Co nanopillar with 20-nm diameter at position ($x = 50$ nm, $y = 50$ nm) [Fig. 4(b), red pulses], and an in-plane spin polarized current is applied along a nanotrack to drive the movement of the skyrmions [Fig. 4(b), blue lines]. After applying a 0.4-ns current pulse with density $J = 5.0 \times 10^{12}$ A/m^2, the magnetization beneath the Co nanopillar switches and results in a skyrmion state [Fig. 4(c), 1], which moves steadily at ~600 m/s under a continuous current of density $J = 1.0 \times 10^{13}$ A/m^2. Thereafter, the chain

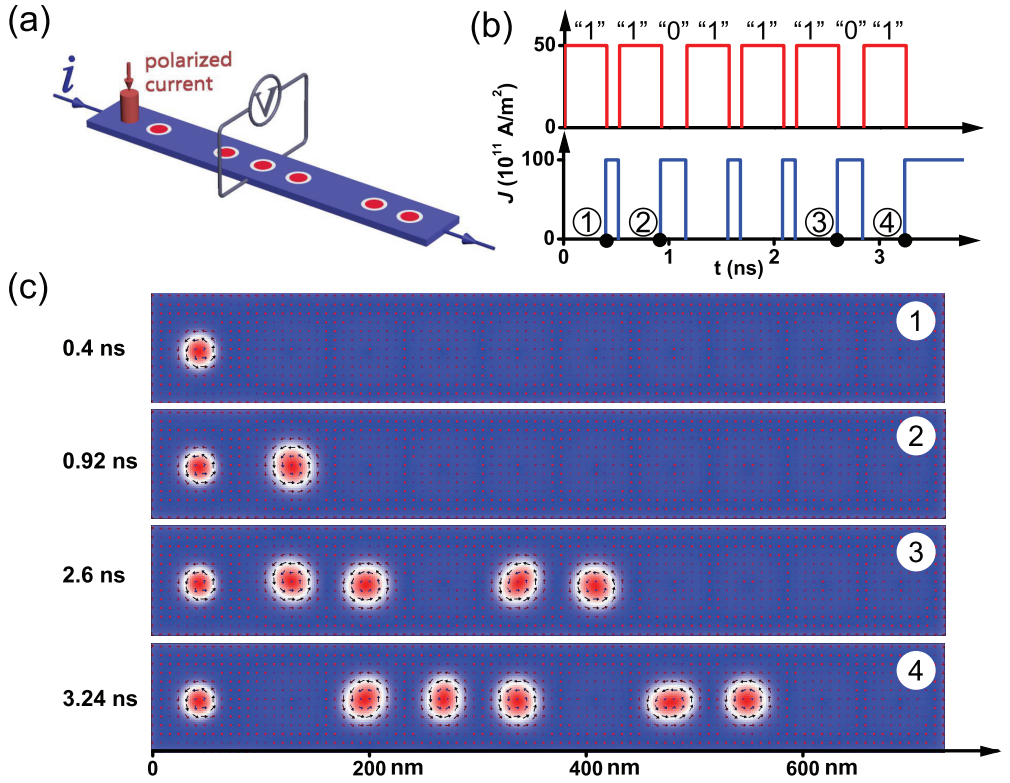

FIG. 4. (a) Schematic of skyrmion race-track memory. (b) Time-dependent current density used for the information encoding. Red current pulse is injected vertically through Co nanopillar to nucleate an isolated skyrmion, and blue steady current is applied along the long axis of the nanotrack to displace the skyrmions. (c) Snapshots of magnetic configuration (top view) in HMS nanotrack at different time sequences, as also noted in (b).

of skyrmions, created by several pulses, moves along the same trajectory as isolated skyrmions with the same velocity [Fig. 4(c), 2]. The nucleation of skyrmion (i.e., writing of information) can be repeated reliably and with given distances [Fig. 4(c), 3]. After six current pulses, we observe a chain of six skyrmions (encoded as "11011101") moving steadily with separate distances along the nanotrack [Fig. 4(c), 4]. Due to the coupling between skyrmion and capping disks, the shape of the moving skyrmion has a slight distortion depending on the relative position with the disks, compared with the static HMS presented in Fig. 2.

In summary, we demonstrate a new concept of hybrid magnetic skyrmion using micromagnetic simulations. By patterning an array of nanodisks onto a magnetic film with DMI, the stability of the skyrmion state can be significantly enhanced due to the coupling from the chiral spins of the vortices above. Also, the skyrmions beneath can move under the action of a spin-polarized current when the vortices are lifted at a certain distance by a nonmagnetic spacer, where the skyrmion Hall effect is effectively suppressed. We also demonstrate a prototype skyrmion-based racetrack memory with reading speed of ~8 Gb/s for a single nanotrack.

This work was supported by the Ministry of Science and Technology of China for the project of Topological magnetic structures and their hetrostructures: physics and devices, and the National Natural Science Foundation of China (Grants No. 51571109, No. 11374145, and No. 51601087) and the Natural Science Foundation of Jiangsu Province (Grant No. BK20150565).

Wu and Miao contribute equally to this work.

[1] U. K. Roszler, A. N. Bogdanov, and C. Pfleiderer, Nature **442**, 797 (2006).

[2] S. Mühlbauer, B. Binz, F. Jonietz, C. Pfleiderer, A. Rosch, A. Neubauer, R. Georgii, and P. Böni, Science **323**, 915 (2009).

[3] X. Z. Yu, Y. Onose, N. Kanazawa, J. H. Park, J. H. Han, Y. Matsui, N. Nagaosa, and Y. Tokura, Nature **465**, 901 (2010).

[4] W. Münzer, A. Neubauer, T. Adams, S. Mühlbauer, C. Franz, F. Jonietz, R. Georgii, P. Böni, B. Pedersen, M. Schmidt, A. Rosch, and C. Pfleiderer, Phys. Rev. B **81**, 041203 (2010).

[5] S. Heinze, K. von Bergmann, M. Menzel, J. Brede, A. Kubetzka, R. Wiesendanger, G. Bihlmayer, and S. Blugel, Nat. Phys. **7**, 713 (2011).

[6] X. Z. Yu, N. Kanazawa, Y. Onose, K. Kimoto, W. Z. Zhang, S. Ishiwata, Y. Matsui, and Y. Tokura, Nat. Mater. **10**, 106 (2011).

[7] O. Petrova and O. Tchernyshyov, Phys. Rev. B **84**, 214433 (2011).

[8] S. X. Huang and C. L. Chien, Phys. Rev. Lett. **108**, 267201 (2012).

[9] T. Schulz, R. Ritz, A. Bauer, M. Halder, M. Wagner, C. Franz, C. Pfleiderer, K. Everschor, M. Garst, and A. Rosch, Nat. Phys. **8**, 301 (2012).

[10] H. Du, J. P. DeGrave, F. Xue, D. Liang, W. Ning, J. Yang, M. Tian, Y. Zhang, and S. Jin, Nano. Lett. **14**, 2026 (2014).

[11] J. Iwasaki, W. Koshibae, and N. Nagaosa, Nano. Lett. **14**, 4432 (2014).

[12] X. Zhang, G. P. Zhao, H. Fangohr, J. P. Liu, W. X. Xia, J. Xia, and F. J. Morvan, Sci. Rep. **5**, 7643 (2015).

[13] T. Schwarze, J. Waizner, M. Garst, A. Bauer, I. Stasinopoulos, H. Berger, C. Pfleiderer, and D. Grundler, Nat. Mater. **14**, 478 (2015).

[14] J. Sampaio, V. Cros, S. Rohart, A. Thiaville, and A. Fert, Nat. Nano. **8**, 839 (2013).

[15] A. Fert, V. Cros, and J. Sampaio, Nat. Nano. **8**, 152 (2013).

[16] N. S. Kiselev, A. N. Bogdanov, R. Schäfer, and U. K. Rößler, J. Phys. D: Appl. Phys. **44**, 392001 (2011).

[17] J. Iwasaki, M. Mochizuki, and N. Nagaosa, Nat. Nano. **8**, 742 (2013).

[18] X. Z. Yu, N. Kanazawa, W. Z. Zhang, T. Nagai, T. Hara, K. Kimoto, Y. Matsui, Y. Onose, and Y. Tokura, Nat. Commun. **3**, 988 (2012).

[19] Y. Tokunaga, X. Z. Yu, J. S. White, H. M. Ronnow, D. Morikawa, Y. Taguchi, and Y. Tokura, Nat. Commun. **6**, 7638 (2015).

[20] G. Chen, A. Mascaraque, A. T. N'Diaye, and A. K. Schmid, Appl. Phys. Lett. **106**, 242404 (2015).

[21] W. Jiang, P. Upadhyaya, W. Zhang, G. Yu, M. B. Jungfleisch, F. Y. Fradin, J. E. Pearson, Y. Tserkovnyak, K. L. Wang, O. Heinonen, S. G. E. te Velthuis, and A. Hoffmann, Science **349**, 283 (2015).

[22] S. Woo, K. Litzius, B. Kruger, M.-Y. Im, L. Caretta, K. Richter, M. Mann, A. Krone, R. M. Reeve, M. Weigand, P. Agrawal, I. Lemesh, M.-A. Mawass, P. Fischer, M. Klaui, and G. S. D. Beach, Nat. Mater. **15**, 501 (2016).

[23] C. Moreau Luchaire, C. Moutafis, N. Reyren, J. Sampaio, C. A. F. Vaz, N. Van Horne, K. Bouzehouane, K. Garcia, C. Deranlot, P. Warnicke, P. Wohlhüter, J. M. George, M. Weigand, J. Raabe, V. Cros, and A. Fert, Nat. Nano. **11**, 444 (2016).

[24] X. Yu, D. Morikawa, Y. Tokunaga, M. Kubota, T. Kurumaji, H. Oike, M. Nakamura, F. Kagawa, Y. Taguchi, T.-h. Arima, M. Kawasaki, and Y. Tokura, Adv. Mater. 1606178 (2017).

[25] L. Sun, R. X. Cao, B. F. Miao, Z. Feng, B. You, D. Wu, W. Zhang, A. Hu, and H. F. Ding, Phys. Rev. Lett. **110**, 167201 (2013).

[26] Y. Y. Dai, H. Wang, P. Tao, T. Yang, W. J. Ren, and Z. D. Zhang, Phys. Rev. B **88**, 054403 (2013).

[27] B. F. Miao, L. Sun, Y. W. Wu, X. D. Tao, X. Xiong, Y. Wen, R. X. Cao, P. Wang, D. Wu, Q. F. Zhan, B. You, J. Du, R. W. Li, and H. F. Ding, Phys. Rev. B **90**, 174411 (2014).

[28] D. A. Gilbert, B. B. Maranville, A. L. Balk, B. J. Kirby, P. Fischer, D. T. Pierce, J. Unguris, J. A. Borchers, and K. Liu, Nat. Commun. **6**, 8462 (2015).

[29] J. Li, A. Tan, K. W. Moon, A. Doran, M. A. Marcus, A. T. Young, E. Arenholz, S. Ma, R. F. Yang, C. Hwang, and Z. Q. Qiu, Nat. Commun. **5**, 4704 (2014).

[30] M. Mochizuki, Phys. Rev. Lett. **108**, 017601 (2012).

[31] B. F. Miao, Y. Wen, M. Yan, L. Sun, R. X. Cao, D. Wu, B. You, Z. S. Jiang, and H. F. Ding, Appl. Phys. Lett. **107**, 222402 (2015).

[32] X. Zhang, Y. Zhou, and M. Ezawa, Nat. Commun. **7**, 10293 (2016).

[33] E. H. Hall, Am. J. Math. **2**, 287 (1879).

[34] J. C. Slonczewski, J. Magn. Magn. Mater. **159**, L1 (1996).

[35] L. Berger, Phys. Rev. B **54**, 9353 (1996).

[36] A. Neubauer, C. Pfleiderer, B. Binz, A. Rosch, R. Ritz, P. G. Niklowitz, and P. Böni, Phys. Rev. Lett. **102**, 186602 (2009).

[37] P. Bruno, V. K. Dugaev, and M. Taillefumier, Phys. Rev. Lett. **93**, 096806 (2004).

[38] M. J. Donahue and D. G. Porter, *OOMMF User's Guide Version 1.0*. (National Institute of Standards and Technology, Gaithersburg, MD, 1999).

[39] X. Fong, OOMMF Oxs extension module of the spin-transfer torque simulations with thermal fluctuations.

[40] N. A. Porter, J. C. Gartside, and C. H. Marrows, Phys. Rev. B **90**, 024403 (2014).

[41] M. Beg, R. Carey, W. Wang, D. Cortés-Ortuño, M. Vousden, M.-A. Bisotti, M. Albert, D. Chernyshenko, O. Hovorka, R. L. Stamps, and H. Fangohr, Sci. Rep. **5**, 17137 (2015).

[42] B. Lebech, J. Bernhard, and T. Freltoft, J. Phys.: Condens. Matter **1**, 6105 (1989).

[43] J. H. Ai, B. F. Miao, L. Sun, B. You, A. Hu, and H. F. Ding, J. Appl. Phys. **110**, 093913 (2011).

[44] M. Yan, A. Kákay, S. Gliga, and R. Hertel, Phys. Rev. Lett. **104**, 057201 (2010).

[45] G. Grinstein and R. H. Koch, Phys. Rev. Lett. **90**, 207201 (2003).

[46] S. Buhrandt and L. Fritz, Phys. Rev. B **88**, 195137 (2013).

[47] A. K. Nandy, N. S. Kiselev, and S. Blügel, Phys. Rev. Lett. **116**, 177202 (2016).

[48] D. A. Garanin, Phys. Rev. B **55**, 3050 (1997).

[49] O. Chubykalo-Fesenko, U. Nowak, R. W. Chantrell, and D. Garanin, Phys. Rev. B **74**, 094436 (2006).

[50] B. Binz and A. Vishwanath, Physica B: Condensed Matter **403**, 1336 (2008).

[51] P. Bruno and C. Chappert, Phys. Rev. Lett. **67**, 1602 (1991).

[52] S. S. P. Parkin, N. More, and K. P. Roche, Phys. Rev. Lett. **64**, 2304 (1990).

[53] S. S. P. Parkin, R. Bhadra, and K. P. Roche, Phys. Rev. Lett. **66**, 2152 (1991).

[54] S. Demokritov, J. A. Wolf, and P. Grünberg, Europhys. Lett. **15**, 881 (1991).

[55] W. Jiang, X. Zhang, G. Yu, W. Zhang, X. Wang, M. Benjamin Jungfleisch, J. E. Pearson, X. Cheng, O. Heinonen, K. L. Wang, Y. Zhou, A. Hoffmann, and S. G. E. te Velthuis, Nat. Phys. **13**, 162 (2017).